

STUDY OF TURBULENT PASSIVE SCALAR DISPERSION WITHIN A REGULAR ARRAY OF OBSTACLES

Bing-Chen Wang, Eugene Yee

Defence Research & Development Canada — Suffield
P.O. Box 4000, Medicine Hat, Alberta, T1A 8K6, Canada
E-mail: bingchen.wang@drdc-rddc.gc.ca, eugene.yee@drdc-rddc.gc.ca

Fue-Sang Lien

Dept. of Mechanical Engineering, University of Waterloo
Waterloo, Ontario, N2L 3G1, Canada
E-mail: fslie@mecheng1.uwaterloo.ca

ABSTRACT

In this paper, we study the turbulent dispersion of a passive scalar released from a transient point source within an obstacle array using an unsteady Reynolds-averaged Navier-Stokes (URANS) method. The numerical results are validated against a set of high-quality water channel measurements. A modification to the modelled transport equation for the turbulence kinetic energy (TKE) is suggested, which leads to significant improvements in the prediction of the TKE levels within and above the obstacle array. The temporal and spatial evolution of the concentration cloud spread is investigated. A new closure model for the scalar dissipation rate is proposed for the transport equation of the concentration variance, and predictions of the concentration variance in a dispersing cloud are compared with the experimental measurements.

INTRODUCTION

The environmental and toxicological impact arising from the dispersion of contaminants (e.g., toxic chemical, biological, or radiological materials) released into the urban environment, where the population density is high, has become an increasingly important problem in recent years. Over the past several years, considerable advances have been made in the physical and numerical modelling of passive scalar dispersion in urban flows. Recent important field studies of urban flow and dispersion include the Mock Urban Setting Trial (MUST) (Biltoft, 2001; Yee and Biltoft, 2004) conducted at U.S. Army Dugway Proving Ground in northwestern Utah in September 2001, and the Joint Urban 2003 Experiment (Allwine et al., 2004) conducted in Oklahoma City, Oklahoma in July 2003. In particular, MUST was designed to provide physical insights into the instantaneous dispersion of an inert tracer through a large regular array of building-like obstacles. The near-field dispersion of a contaminant cloud in the MUST array has been physically modelled in a wind tunnel simulation at 1:50 scale (Gailis and Hill, 2006), in a water channel simulation at 1:205 scale (Yee et al., 2006; Gailis et al., 2007), and numerically modelled using a RANS approach (Hsieh et al., 2007). In this paper, we apply a URANS method to numerically simulate the dispersion of a tracer released from a transient point source within the MUST array, and compare the model predictions with detailed measurements provided by a water channel simulation (Yee et al., 2006).

In order to establish a reliable numerical model for de-

scribing the transport and dispersion of a passive scalar, it is necessary to understand the micro-mixing processes of the scalar and to be able to quantify the rate at which the small-scale scalar fluctuation is destroyed through molecular diffusion. To this purpose, it is of great research interest to study the transport of the scalar variance. Warhaft and Lumley (1978) and Bégulier et al. (1978) studied the ratio between the dissipation time scale for the scalar variance and the integral time scale for the turbulent flow field. Fackrell and Robins (1982) and Sykes et al. (1984) investigated the scalar dissipation length scale for modelling scalar variance transport for the case of a point source release. Hsieh et al. (2007) proposed an explicit semi-empirical algebraic scalar dissipation length scale model for studying concentration variance. In this study, we propose an alternative explicit semi-empirical algebraic dissipation length scale model for studying concentration variance.

EXPERIMENTAL AND NUMERICAL APPROACHES

In this section, we first describe the physical modelling of the MUST array conducted in a water channel simulation, and then describe the numerical algorithm for simulating the dispersion of a tracer released from a transient point source within the obstacle array. Finally, we propose a new scalar dissipation length scale for concentration variance.

Physical modelling and water channel measurements

The water channel simulations of flow and dispersion in the MUST array were conducted at Coanda R&D Corporation (Burnaby, BC, Canada). The test section of the water channel was 10 m \times 1.5 m \times 0.9 m in the streamwise (x), spanwise (y) and wall-normal (z) directions, respectively. The dimension of the MUST obstacle was $L \times W \times H = 2.42 \text{ m} \times 12.2 \text{ m} \times 2.54 \text{ m}$ in the original full-scale field test (Biltoft, 2001; Yee and Biltoft, 2004). A physical model of the MUST array at 1:205 scale was used in the water channel experiments [see Fig. 1 for a photograph of the physical model of the MUST array and Figs. 2(a) and (b) for a description of its geometry]. The Reynolds number of the flow in the water channel simulation was approximately $Re_H = 4700$ [based on the free stream velocity $U_b = 0.38 \text{ m s}^{-1}$ and obstacle height $H = 1.05L$, where $L = 11.8 \text{ mm}$ (at a 1:205 scale) is the length of the obstacle used in water channel simulation]. In our analysis of the experimental results and numerical simulations, flow quantities were non-dimensionalized using U_b and L (implying that the time scale for non-dimensionalization was $t_s = L/U_b = 0.031 \text{ s}$). As

shown in Figs. 2(a) and (b), the ground-level point source was located at row 1.5 (midway between the first and second rows of the obstacle array) along the centerline ($y/L = 0$) of the fifth column of obstacles. The diameter of the point source was $d_0 = 2.8$ mm. The duration of the puff released from the point source was 1.25 s, and during this period of time a fluorescein dye (tracer) was released at a volume flow rate of 24 ml min^{-1} . A series of 100 individual puffs was released in each experiment, enabling ensemble-averaged cloud concentration statistics to be obtained.

The velocity field was measured using a 4-beam 2-component TSI fibre-optic laser doppler anemometer (LDA) powered by an argon-ion laser. Titanium dioxide particles were used as seed particles. The velocity data were collected with a frequency ranging from 50 to 500 Hz and a sampling time of 500 seconds was used at each measurement location.

The concentration field was measured using a laser induced fluorescence (LIF) linescan system. The linescan LIF system allows simultaneous multi-point concentration measurements to be made along the laser beam. Here, sodium fluorescent dye was used as the tracer and was illuminated using an argon-ion laser. The intensity of this illumination was measured using a Dalsa monochrome digital linescan CCD camera with 12-bit amplitude resolution (4096 digitization levels) at a rate of 300 lines per seconds. The total sampling time for each measurement position was 1000 seconds. Each linescan consisted of 1024 pixels, which gave a spatial resolution of between about 0.5 to 1 mm in the spanwise direction.

Governing equations and numerical algorithm

The flow and concentration fields are described by the conservation laws of mass, momentum and concentration for a neutrally-stratified incompressible flow expressed in the usual Reynolds-averaged form. In addition to these conservation laws, the transport equations for TKE k , the rate of dissipation ϵ of TKE and concentration variance $\overline{c'^2}$ are also used. These governing equations assume the following form in a Cartesian coordinate system:

$$\frac{\partial \bar{u}_i}{\partial x_i} = 0, \quad (1)$$

$$\frac{\partial \bar{u}_i}{\partial t} + \frac{\partial (\bar{u}_i \bar{u}_j)}{\partial x_j} = -\frac{\partial \bar{p}}{\partial x_i} + \frac{\partial}{\partial x_j} \left(\nu \frac{\partial \bar{u}_i}{\partial x_j} \right) - \frac{\partial \overline{u'_i u'_j}}{\partial x_j}, \quad (2)$$

$$\frac{\partial k}{\partial t} + \frac{\partial (\bar{u}_j k)}{\partial x_j} = \frac{\partial}{\partial x_j} \left[\left(\nu + \frac{\nu_t}{\sigma_k} \right) \frac{\partial k}{\partial x_j} \right] + P_k - C_{\epsilon 0} \epsilon, \quad (3)$$

$$\frac{\partial \epsilon}{\partial t} + \frac{\partial (\bar{u}_j \epsilon)}{\partial x_j} = \frac{\partial}{\partial x_j} \left[\left(\nu + \frac{\nu_t}{\sigma_\epsilon} \right) \frac{\partial \epsilon}{\partial x_j} \right] + \frac{\epsilon}{k} (C_{\epsilon 1} P_k - C_{\epsilon 2} \epsilon), \quad (4)$$

$$\frac{\partial \bar{c}}{\partial t} + \frac{\partial (\bar{u}_j \bar{c})}{\partial x_j} = \frac{\partial}{\partial x_j} \left(D \frac{\partial \bar{c}}{\partial x_j} \right) - \frac{\partial \overline{u'_j c'}}{\partial x_j} + S, \quad (5)$$

$$\frac{\partial \overline{c'^2}}{\partial t} + \frac{\partial (\bar{u}_j \overline{c'^2})}{\partial x_j} = \frac{\partial}{\partial x_j} \left(D \frac{\partial \overline{c'^2}}{\partial x_j} - \overline{u'_j c'^2} \right) - 2 \overline{u'_j c'} \frac{\partial \bar{c}}{\partial x_j} - \epsilon_c. \quad (6)$$

Here, \bar{c} is the mean concentration, S is the source density of the tracer, D is the molecular diffusivity, ν is the kinematic viscosity of the fluid, and $\nu_t \stackrel{\text{def}}{=} C_\mu k^2 / \epsilon$ is the kinematic eddy viscosity. The closure constants are given as follows: $C_\mu = 0.09$, $\sigma_k = 1.0$, $\sigma_\epsilon = 1.3$, $C_{\epsilon 1} = 1.44$ and $C_{\epsilon 2} = 1.92$. The Reynolds stresses are modelled using the conventional linear eddy-viscosity assumption:

$$\overline{u'_i u'_j} = \frac{2}{3} k \delta_{ij} - \nu_t \left(\frac{\partial \bar{u}_i}{\partial x_j} + \frac{\partial \bar{u}_j}{\partial x_i} \right). \quad (7)$$

In Eqs. (5) and (6), the turbulent fluxes of concentration and concentration variance are modelled using the standard

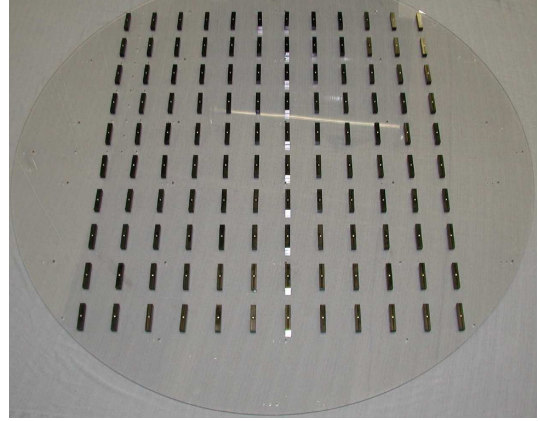


Fig. 1: MUST array in water channel.

gradient diffusion hypothesis, which take the following forms

$$\overline{u'_j c'} = -\frac{\nu_t}{\sigma_c} \frac{\partial \bar{c}}{\partial x_j} \quad \text{and} \quad \overline{u'_j c'^2} = -\frac{\nu_t}{\sigma_c} \frac{\partial \overline{c'^2}}{\partial x_j}, \quad (8)$$

respectively. Here, σ_c is the turbulent Schmidt number set to 0.9.

Equations (1)–(4) represent the standard k - ϵ model for predicting the turbulent flow field, except that an additional coefficient $C_{\epsilon 0}$ is incorporated into the k -equation to adjust the balance between production and dissipation of TKE. It has been confirmed by some previous investigations (Lien and Yee, 2004; Hsieh et al., 2007) that the standard k - ϵ approach tends to underpredict the TKE levels for flows over obstacle arrays. In the next section, we will compare the predictions for TKE obtained using two different values of $C_{\epsilon 0}$; namely, 1.0 corresponding to the standard k - ϵ model and 0.7 for our modified model. We will demonstrate that this simple empirical modification of the k -equation is effective for improving prediction of TKE levels in obstacle arrays in comparison to those provided by the standard k - ϵ model.

The numerical simulations were performed using two self-developed computer codes: urbanSTREAM and urbanEU. Here, urbanSTREAM is a general curvilinear second-order accurate fully conservative and implicit finite-volume code designed for the numerical simulation of urban flow; and, urbanEU is an Eulerian grid urban dispersion model based on the numerical solution of a K -theory advection-diffusion equation (Yee et al., 2007). The flow solver for urbanSTREAM is based on numerical algorithms described by Lien and Leschziner (1994a). The SIMPLE algorithm was used for pressure correction and checkerboard oscillations in the pressure field arising from a state of pressure-velocity decoupling on a collocated grid were removed using the momentum interpolation scheme described by Rhie and Chow (1983). Convective fluxes at the faces of a control volume were approximated using a second-order accurate total-variation-diminishing (TVD) scheme (Lien and Leschziner, 1994b) implemented using a deferred correction method.

At the inlet, Dirichlet boundary conditions were used for both the flow and concentration fields. The inlet flow conditions were obtained from the experimental measurements, and the values of concentration and concentration variance at the inlet were set to zero. At every solid boundary surface, no-slip and impermeability wall boundary conditions were applied for the flow field (mean velocity and turbulence quantities k and ϵ), and zero-flux boundary conditions were used for the concentration and concentration variance fields.

As shown in Figs. 2(b) and (c), the grid lines have been refined close to the source location and near every solid surface. At every solid surface, the generalized wall function proposed by Kim (1995) was applied, which is dependent on the local pressure gradients and the non-equilibrium flow state, and thus, constitutes a useful near-wall treatment for a complex flow which potentially can involve separation, recirculation and reattachment. For all flow variables, zero-flux boundary conditions were applied at the upper free surface of the computational domain, fully developed boundary conditions were used at the outlet, and periodic boundary conditions were applied in the spanwise direction.

A total time of 20 seconds was simulated using URANS with a temporal resolution of 0.04 seconds per time step. In this study, two different grids and computational domains were used in order (i) to determine if the computed solution was grid-independent, (ii) to investigate the sensitivity of the predicted concentration and concentration variance fields with respect to the degree of resolution of the small point source used in the experiments, (iii) to accurately quantify the temporal and spatial evolution of the cloud centroid and spread, and (iv) to investigate the sensitivity of the scalar variance dissipation model to the size of the computational domain. For this purpose, the non-dimensional size for the large and small computational domains used in this study were, respectively, as follows: $685.6L \times 41.5L \times 60L$ and $105.6L \times 41.5L \times 30L$, with $224 \times 53 \times 30$ and $264 \times 119 \times 42$ control volumes (in the streamwise, spanwise, and wall-normal directions, respectively). Both the large and small computational domains tested in the simulation include 12 rows and 5 central columns of obstacles. An upstream fetch of $15L$ (distance between the inlet plane and the windward face of the first row of obstacles) was used for both the large and small computational domains. The major difference between these two computational domains lay in the extent of the downstream fetch between the last row of obstacles and the outlet plane.

Scalar variance dissipation model

In order to close Eq. (6), the concentration variance dissipation rate $\epsilon_c \stackrel{\text{def}}{=} 2D \frac{\partial c'}{\partial x_j} \frac{\partial c'}{\partial x_j}$ needs to be modelled. One of the most popular methods for this closure is to assume that the dissipation time scale (t_{ec}) that is characteristic of those eddy motions that destroy the scalar variance c'^2 is proportional to the integral time scale ($t_\epsilon = k/\epsilon$) of the turbulent flow. In this case, ϵ_c can be modelled as

$$\epsilon_c = C_{\chi_1} \frac{1}{t_{ec}} c'^2 = C_{\chi_1} \frac{\epsilon}{k} c'^2. \quad (9)$$

The value of the closure constant C_{χ_1} varies in the literature and is usually set to 2 following the suggestion of Béguyer et al. (1978). The turbulent length scale of the flow field corresponding to t_ϵ is evaluated as $\Lambda_k = k^{3/2}/\epsilon$.

For the case of a transient puff release from a point source, there are two stages of diffusion; namely, the initial or meandering phase where the cloud length scale Λ is smaller than the dominant large (energy containing) eddies and the cloud meanders due to the motion of large eddies, and the late phase where Λ grows bigger than the length scale of the large eddies and the cloud spreads with constant diffusivity (Sykes et al., 1984). In general, the model represented by Eq. (9) cannot correctly represent the scalar dissipation in the early meandering stage of cloud diffusion, because Λ for a very compact source is generally much smaller than the integral length scale Λ_k of turbulence in the initial stage of

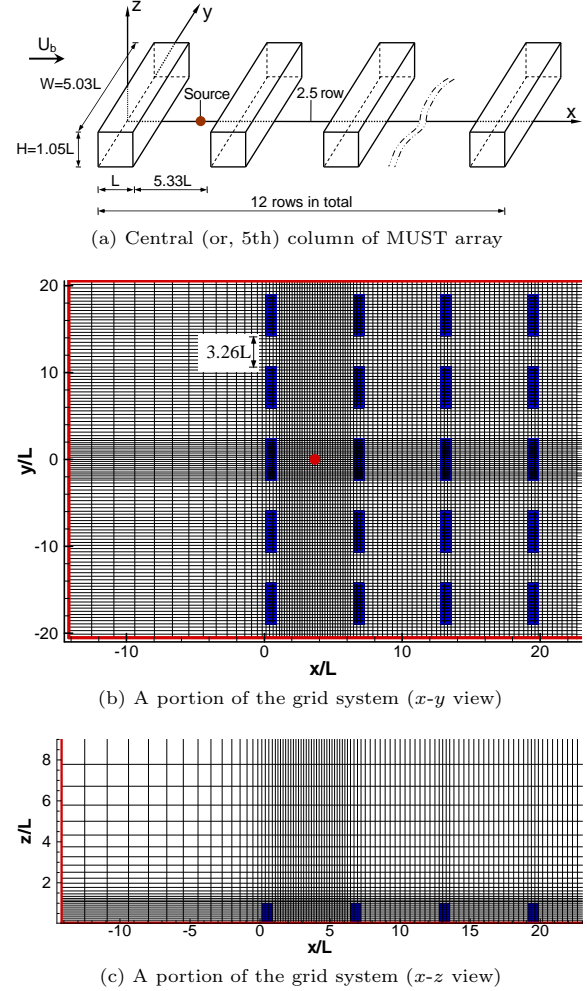


Fig. 2: Geometry of the MUST array for the small computational domain ($L = 11.8$ mm).

cloud development. From these considerations, Fackrell and Robins (1982) proposed an alternative model in which the scalar dissipation length scale Λ_c is represented as follows:

$$\epsilon_c = C_{\chi_2} \frac{k^{1/2}}{\Lambda_c} c'^2. \quad (10)$$

The key issue in this model is the determination of the value of Λ_c . Sykes et al. (1984) proposed an ordinary differential equation for quantifying the temporal evolution of Λ_c . Hsieh et al. (2007) evaluated Λ_c using the “size” of the cloud defined as the geometric mean of the cloud spreads in the three coordinate directions:

$$\Lambda_{c3D} = \Lambda_{c3D}(t) = (\sigma_x(t)\sigma_y(t)\sigma_z(t))^{1/3}, \quad (11)$$

where $\sigma_x(t)$, $\sigma_y(t)$ and $\sigma_z(t)$ are the cloud spreads in the x -, y -, and z -directions, respectively, at time t after the release. For example, the streamwise cloud spread is defined as

$$\sigma_x(t) = \left(\frac{\iiint (x - \bar{x})^2 \bar{c}(x, y, z, t) dx dy dz}{\iiint \bar{c}(x, y, z, t) dx dy dz} \right)^{1/2}, \quad (12)$$

where the streamwise cloud centroid is

$$\bar{x} = \bar{x}(t) = \frac{\iiint x \bar{c}(x, y, z, t) dx dy dz}{\iiint \bar{c}(x, y, z, t) dx dy dz}. \quad (13)$$

Figures 3 and 4 show the temporal and spatial evolution of the cloud centroid and spreads calculated using the large computational domain. It is seen from these two figures that

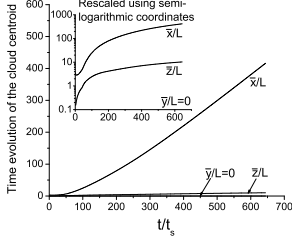


Fig. 3: Time evolution of the cloud centroid.

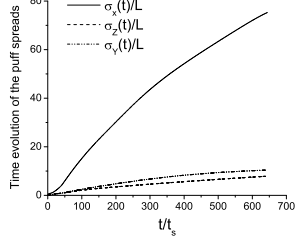


Fig. 4: Time evolution of the cloud spread along the three coordinate directions.

the cloud centroid and spreads in the streamwise direction evolve at a rate that is at least one order of magnitude larger than those in the spanwise and wall-normal directions. The cloud is greatly stretched/enlongated in the streamwise direction in comparison with the other two directions. What this implies is that for the small computational domain, the leading edge of the cloud is already at or beyond the outflow plane of the computational domain by the time the streamwise component of the cloud centroid “arrives” at the last row of obstacles (which occurs at approximately 5.6 s after the release). To avoid this undesirable condition (whereby the streamwise dimensions of the cloud may be distorted owing to an insufficient downstream fetch in the computational domain), we modified Eq. (11) to determine the “size” of the cloud based on only the spanwise and wall-normal cloud spreads, viz.

$$\Lambda_{c2D} = \Lambda_{c2D}(x, t) = (\sigma_y(x, t)\sigma_z(x, t))^{1/2}, \quad (14)$$

where the cloud spreads $\sigma_y(x, t)$ and $\sigma_z(x, t)$ are evaluated locally in the vertical y - z plane. The spanwise cloud (puff) spread $\sigma_y(x, t)$ is determined as

$$\sigma_y(x, t) = \left(\frac{\iint (y - \bar{y})^2 \bar{c}(x, y, z, t) dy dz}{\iint \bar{c}(x, y, z, t) dy dz} \right)^{1/2}, \quad (15)$$

with the spanwise cloud centroid in the local y - z plane evaluated as

$$\bar{y} = \bar{y}(x, t) = \frac{\iint y \bar{c}(x, y, z, t) dy dz}{\iint \bar{c}(x, y, z, t) dy dz}. \quad (16)$$

The expression for $\sigma_z(x, t)$ is analogous to Eq. (15).

The proposed model for concentration variance dissipation derives from the general form of Eq. (10), which is

$$\epsilon_c = \frac{k^{1/2}}{\Lambda_c} c'^2. \quad (17)$$

with Λ_c being defined as

$$\Lambda_c = \Lambda_c(x, t) = \max \left[\Lambda_0, \min \left(\frac{\Lambda_{c2D}}{C_{\chi 21}}, \frac{\Lambda_{k2D}}{C_{\chi 22}} \right) \right]. \quad (18)$$

Here, $C_{\chi 21} = C_{\chi 22} = 1.5$ are two model constants, and Λ_0 is the initial puff size taken as $\Lambda_0 = d_0/2$. This model ensures that the scalar dissipation scale Λ_c is greater than or comparable to the initial source size (as it must be), and also avoids any potential numerical instability (such as if $\Lambda_c \rightarrow 0$) in Eq. (17). Also in Eq. (18), Λ_{k2D} is the integral length scale of turbulence averaged over a vertical cross-section of the cloud, viz.

$$\Lambda_{k2D} = \Lambda_{k2D}(x, t) = \frac{\iint \Lambda_k \bar{c}(x, y, z, t) dy dz}{\iint \bar{c}(x, y, z, t) dy dz}. \quad (19)$$

Equation (18) also ensures that the dissipation length scale for concentration variance is associated with eddies smaller than the local cloud size (characterized by Λ_{c2D}) at the initial meandering stage, and is limited by the integral length

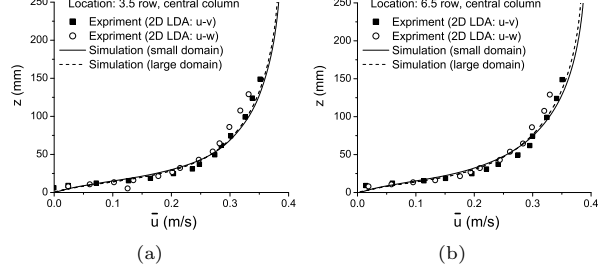


Fig. 5: Mean velocity profile at two different streamwise locations.

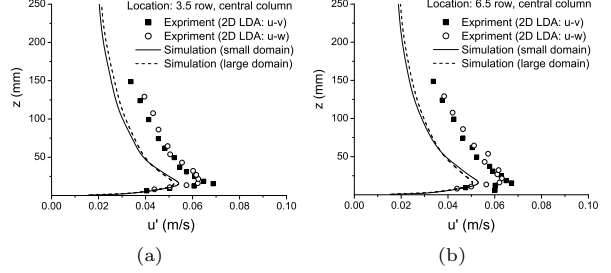


Fig. 6: Streamwise turbulence intensity at two different streamwise locations (obtained using $C_{\epsilon 0} = 1.0$).

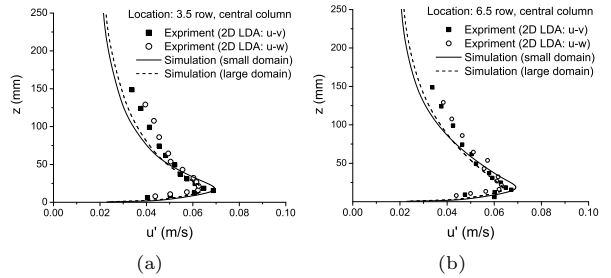


Fig. 7: Streamwise turbulence intensity at two different streamwise locations (obtained using $C_{\epsilon 0} = 0.7$).

scale of turbulence (characterized by Λ_{k2D}) when the cloud spread becomes larger than the energy containing eddies of the flow in the second stage of cloud diffusion.

RESULTS AND ANALYSIS

In this section, we analyze the predicted results on the flow and concentration fields and compare them with the water channel measurements. Owing to page limitations, we will only display and discuss the predicted and measured fields at row 3.5 and row 6.5 along the central column of obstacles. For the concentration and concentration variance fields, we will also display and discuss the predicted and measured field properties at two different heights; namely, at $z/H = 0.75$ within the canopy and at $z/H = 1.5$ above the canopy.

Figures 5(a) and (b) compare the predicted mean velocity profiles with two sets of 2-D LDA measurements (i.e., the u - v components and u - w components) at two different streamwise locations. As can be seen from these figures, the agreement between the predicted and experimental results is excellent. Figures 6 and 7 show the predicted streamwise velocity standard deviations, or, root-mean square (rms) values [$u'_{rms} \stackrel{\text{def}}{=} (\overline{u'u'})^{1/2}$] for two different choices of $C_{\epsilon 0}$ [cf. Eq. (3)]. As seen in Fig. 6, for the standard k - ϵ approach with $C_{\epsilon 0} = 1.0$, u'_{rms} is significantly underpredicted (by approximately 30%), an observation that is consistent with the results of Hsieh et al. (2007) based on the steady RANS ap-

proach. Figure 7 is obtained using $C_{\epsilon 0} = 0.7$ based on the modified k -equation, which shows a significant improvement in the predicted levels of u'_{rms} . An explanation for this improvement is that the closure coefficient $C_{\epsilon 0}$ compensates for the deficiency in the linear eddy viscosity assumption for modelling of the Reynolds stress tensor. Although slight differences exist, the mean and rms streamwise velocity predicted using the large and small computational domains are in good agreement as shown in Figs. 5–7, suggesting that we have obtained a grid-independent solution for the flow field. Figure 8 displays the complex pattern of vortex shedding, which is visualized here using the normalized mean spanwise velocity within the obstacle array (obtained on the small computational domain). From the figure, it is observed that when the flow passes by an obstacle, symmetrical vortical structures are generated, and these vortical structures are much larger at the front and rear edges of the array than inside the array where the size of the flow structures are inhibited due to the presence of the obstacles.

Figure 9 displays the isopleths for the cloud dosage $\mathcal{D}(t) \stackrel{\text{def}}{=} \int_0^t \bar{c} dt$, normalized using the source concentration c_s . As expected, the figure shows that the dosage is the greatest along the central ($y/L = 0$) column and/or closer to the source location ($x/L = 3.665$). As the distance from the central column increases (i.e., $|y/L|$ increases), the dosage decreases. In fact, the dosage field of the dispersing cloud within the obstacle array possesses a Gaussian distribution. This feature is further demonstrated in Figs. 10(a)–(d), which exhibit the lateral distribution of the normalized dosage at different downstream locations. By comparing Fig. 10(a) with 10(b) and Fig. 10(c) with 10(d), it is evident that the dosage is more widely distributed in the downwind location (row 6.5) in comparison with that in the upwind location (row 3.5). By comparing Fig. 10(a) with 10(c) and Fig. 10(b) with 10(d), it is observed that the dosage level within the canopy ($z/H = 0.75$) is, in general, larger than that above the canopy ($z/H = 1.5$). This observation is consistent with the physical process that after the puff is released into the flow from the ground-level point source, the size of the cloud grows and the cloud centroid increases in height as the flow sweeps material around and over the obstacles in the downwind direction. In our numerical simulations, we observed that the lateral distribution of the dosage is influenced significantly by the Schmidt number σ_c used in the model. Furthermore, if values for σ_c were restricted within the interval $[0.9, 1.0]$, the predicted dosages were generally in good agreement with the experimental measurements as is evident in Fig. 10 (obtained using $\sigma_c = 0.9$).

Figures 11(a)–(d) compare the predicted and measured results for the temporal development of the normalized mean concentration \bar{c}/c_s at different locations. In general, it is observed that the instantaneous peak value of the normalized concentration is overpredicted by the numerical simulations in comparison with the experimental data. Figures 12(a)–(d) compare the normalized concentration standard deviation $(\overline{c'^2})^{1/2}/c_s$ predicted by the simulations with the experimental measurements. Although the level of $(\overline{c'^2})^{1/2}/c_s$ is generally well predicted, it is observed that the predicted time of the peak value occurs earlier (by about 1 s) relative to that seen in the measurements. Considering an uncertainty of ± 0.5 s in the determination of the exact release time of the puff, this discrepancy between the predicted and observed values is not significant.

From Figs. 10–12, it is confirmed that we have obtained a

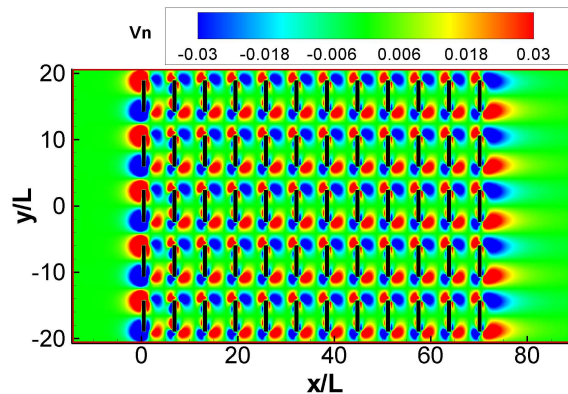


Fig. 8: Vortex shedding visualized using the normalized spanwise velocity $v_n \stackrel{\text{def}}{=} \bar{v}/U_b$ (at the height $z/H = 0.61$).

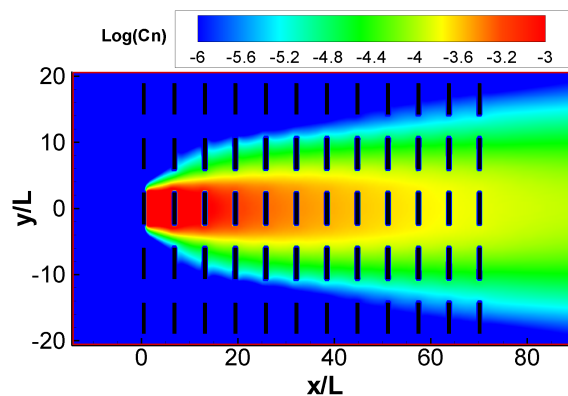


Fig. 9: Puff cloud visualized using normalized dosage $c_n \stackrel{\text{def}}{=} \mathcal{D}(t)/c_s$ isopleths displayed on a logarithmic scale at $t = 20$ s (at the height $z/H = 0.61$).

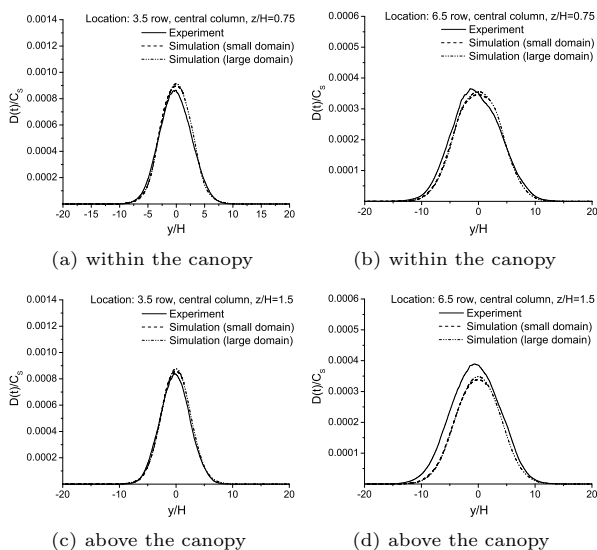


Fig. 10: Normalized puff dosage $\mathcal{D}(t)/c_s$ at $t = 20$ s at two different streamwise locations.

grid-independent solution for the concentration and concentration variance fields, because little difference can be seen between the predictions obtained using the large and small computational domains. Also, it should be noted that for the dispersion results shown here (both predicted and measured), the concentration and concentration variance fields are insensitive to the precise source location and size of the

control volume used for representing the source, as long as the source was situated within the large recirculation zone on the lee side of the obstacle. The large recirculating eddy behind the obstacle mixes the tracer from the source rapidly into the recirculation bubble, and in so doing, smears out any differences in the treatment of the precise location and size of the point source.

CONCLUSIONS AND DISCUSSIONS

The transient release of a passive tracer from a ground-level point source in the MUST array has been studied using a URANS method. In comparison with water channel measurements, the numerical simulation has successfully predicted the velocity, TKE, concentration and concentration variance fields. The proposed modification to the k -equation within the standard k - ϵ model is effective for improving the prediction of the TKE levels. However, whether this modification is necessary for alternative k - ϵ approaches (e.g., use of implicit or explicit nonlinear algebraic models for the Reynolds stress tensor) for the simulation of MUST dispersion is a subject for future investigation. The proposed dissipative length scale model is insensitive to the size of the computational domain in the streamwise direction, it is capable of reflecting the mechanism of the two stages of cloud dispersion for the transient release of a passive scalar from a point source, and it has also been demonstrated to be capable of correctly simulating the transport of concentration variance for the MUST dispersion test case. Although the test results are encouraging, the model proposed here still needs to be further validated using a number of different test cases of obstacle arrays.

REFERENCES

Allwine, K. J., Leach, M. J., Stockham, L. W., Shinn, J. S., Hosker, R. P., Bowers, J. F., and Pace, J. C., 2004, "Overview of Joint Urban 2003—An atmospheric dispersion study in Oklahoma City". *Symposium on Planning, Nowcasting, and Forecasting in the Urban Zone*, Seattle Washington, American Meteorol. Soc.

Béguier, C., Dekeyser, I., and Launder, B. E., 1978, "Ratio of scalar and velocity dissipation time scales in shear flow turbulence", *Phys. Fluids*, vol. 21, pp. 307–310.

Biltoft, C. A., 2001, "Customer report for Mock Urban Setting Test", DPG Document No. WDTC-FR-01-121. Technical report, West Desert Test Center, U.S. Army Dugway Proving Ground, Dugway, Utah. 58 pages.

Fackrell, J. E. and Robins, A. G., 1982, "Concentration fluctuations and fluxes in plumes from point sources in a turbulent boundary layer", *J. Fluid Mech.*, vol. 117, pp. 1–26.

Gailis, R. M. and Hill, A., 2006, "A wind-tunnel simulation of plume dispersion within a large array of obstacles", *Boundary-Layer Meteorol.*, vol. 119, pp. 289–338.

Gailis, R. M., Hill, A., Yee, E., and Hilderman, T., 2007, "Extension of a fluctuating plume model of tracer dispersion to a shear boundary layer and to a large array of obstacles", *Boundary-Layer Meteorol.* vol. 122, pp. 577–607.

Hsieh, K. J., Lien, F.-S., and Yee, E., 2007, "Numerical modeling of scalar dispersion in an urban canopy layer", *J. Wind Eng. Ind. Aerodyn.* (in press).

Kim, S.-E., 1995, "A near-wall treatment using wall functions sensitized to pressure gradient", *ASME FED: Separated and Complex Flows*, vol. 217, pp. 273–280.

Lien, F.-S. and Leschziner, M. A., 1994a, "A general non-orthogonal collocated finite volume algorithm for turbulent flow at all speeds incorporating second-moment turbulence-transport closure, Part 1: computational implementation", *Comput. Meth. Appl. Mech. Eng.*, vol. 114, pp. 123–148.

Lien, F.-S. and Leschziner, M. A., 1994b, "Upstream monotonic interpolation for scalar transport with application to complex turbulent flows", *Int. J. Numer. Meth. Fluids*, vol. 19, pp. 527–548.

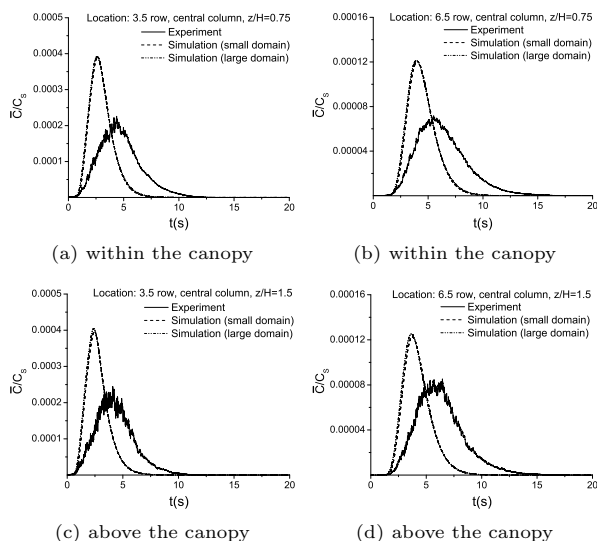


Fig. 11: Time evolution of the cloud concentration at two different streamwise locations.

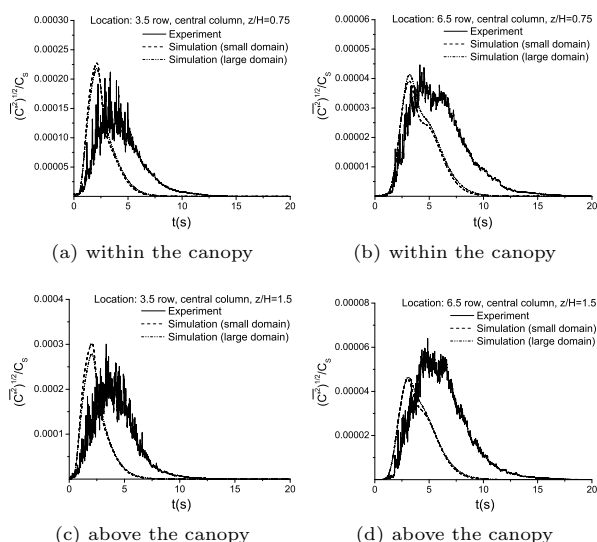


Fig. 12: Time evolution of the concentration variance at two different streamwise locations.

Lien, F.-S. and Yee, E., 2004, "Numerical modelling of the turbulent flow developing within and over a 3-D building array, part I: a high-resolution Reynolds-averaged Navier-Stokes approach", *Boundary-Layer Meteorol.*, vol. 112, pp. 427–466.

Rhie, C. M. and Chow, W. L., 1983, "Numerical study of the turbulent flow past an isolated airfoil with trailing edge separation", *AIAA J.*, vol. 21, pp. 1525–1532.

Sykes, R. I., Lewellen, W. S., and Parker, S. F., 1984, "A turbulent-transport model for concentration fluctuations and fluxes", *J. Fluid Mech.*, vol. 139, pp. 193–218.

Yee, E. and Biltoft, C. A., 2004, "Concentration fluctuation measurements in a plume dispersing through a regular array of obstacles", *Boundary-Layer Meteorol.*, vol. 111, pp. 363–415.

Yee, E., Gailis, R. M., Hill, A., Hilderman, T., and Kiel, D., 2006, "Comparison of wind-tunnel and water-channel simulations of plume dispersion through a large array of obstacles with a scaled field experiment", *Boundary-Layer Meteorol.* vol. 121, pp. 389–432.

Yee, E., Lien, F. S., and Ji, H., 2007, Technical Description of Urban Microscale Modeling System: Component 1 of CRTI Project 02-0093RD, DRDC Suffield TR 2007-067, Defence R&D Canada – Suffield, 55 pages.

Warhaft, Z. and Lumley, J. L., 1978, "An experimental study of the decay of temperature fluctuations in grid-generated turbulence", *J. Fluid Mech.*, vol. 88, pp. 659–684.